J|A|C|S
ARTICLES
Published on Web 03/02/2004

Crystal Structure and Microstructure of Some $La_{2/3-x}Li_{3x}TiO_3$ Oxides: An Example of the Complementary Use of Electron Diffraction and Microscopy and Synchrotron X-ray Diffraction To Study Complex Materials

Susana García-Martín,[†] Miguel A. Alario-Franco,[†] Helmut Ehrenberg,[‡] Juan Rodríguez-Carvajal,[§] and Ulises Amador*,[||]

Contribution from the Departamento de Química Inorgánica, Facultad de Ciencias Químicas, Universidad Complutense, 28040- Madrid, Spain, Materials Science, Darmstadt University of Technology, Petersenstrasse 23, D-64287 Darmstadt, Germany, Laboratoire Léon Brillouin (CEA-CNRS) Centre d'Etudes de Saclay, 91191 Gif-sur-Yvette Cedex, France, and Departamento de Ciencias Químicas, Facultad de Ciencias Experimentales y de la Salud, Universidad San Pablo-CEU, Urbanización Montepríncipe, 28668-Boadilla del Monte, Madrid, Spain

Received September 9, 2003; E-mail: uamador@ceu.es

Abstract: Three representative oxides of the $La_{2/3-x}Li_{3x}TiO_3$ system have been studied by selected area electron diffraction (SAED), high-resolution transmission electron microscopy (HRTEM), and powder synchrotron X-ray diffraction. HRTEM showed that the materials have a complex microstructure. The SAED and HRTEM results have allowed us to propose a model to refine the crystal structure of these oxides that also accounts for their microstructure. The materials have a perovskite-related structure with a diagonal unit cell ($\sqrt{2}a_p \times \sqrt{2}a_p \times 2a_p$) as a consequence of the tilting of the TiO_6 octahedra. Ordering of lanthanum and lithium ions and vacancies along the $2a_p$-axis, as well as displacements of titanium ions from the center of the octahedra, have been determined. The size and shape of the domains have been obtained from the synchrotron X-ray diffraction data; in addition, other extended defects such as strains and compositional fluctuations have been detected.

Introduction

Materials of the general formula $La_{2/3-x}Li_{3x}TiO_3$ with perovskite-related structure are among the best Li^+-ion conductors known to date and are, therefore, promising candidates as solid-state electrolytes for lithium secondary batteries. A great amount of studies on this system have been found in the literature since Inaguma et al. reported in 1993 a very high value of lithium conductivity in $La_{0.5}Li_{0.34}TiO_{2.94}$ ($\sigma = 1 \times 10^{-3}$ S cm^{-1} at room temperature).[1] The stoichiometry range of the solid solution was determined,[2,3] and the electrical properties of these materials were soon well established.[2,4−6] However, their detailed crystal structure has not been properly determined yet, as can be concluded from the abundant amount of controversial results published in the literature.

$La_{0.5}Li_{0.5}TiO_3$ was first reported as a cubic perovskite with lithium and lanthanum ions disordered within the A-sites.[7,8] Further papers suggested a tetragonal tungsten bronze type of structure for this oxide.[9,10]

Weak superlattice reflections with respect to the cubic perovskite structure were detected in the X-ray diffraction pattern of the $La_{0.5}Li_{0.34}TiO_{2.94}$.[1] Thus, a tetragonal perovskite-based structure with unit cell $a_p \times a_p \times 2a_p$ (p refers to the cubic perovskite-type structure), in which Li^+ and La^{3+} ions were ordered along the *c*-axis, was proposed.

On the other hand, electron diffraction and high-resolution transmission electron microscopy studies on $La_{0.5}Li_{0.5}TiO_3$[11] have suggested a different tetragonal unit cell ($a = b \approx \sqrt{2}a_p$, $c \approx 2a_p$).

Fourquet et al. have also studied the $La_{2/3-x}Li_{3x}TiO_3$ system by electron diffraction and microscopy in addition to Rietveld refinement of the powder X-ray diffraction patterns of some of these oxides.[12] They have again proposed a tetragonal unit cell ($a \approx a_p$, $c \approx 2a_p$) and a structural model based on the *P*4/*mmm*

[†] Universidad Complutense.
[‡] Darmstadt University of Technology.
[§] Laboratoire Léon Brillouin (CEA-CNRS) Centre d'Etudes de Saclay.
[||] Universidad San Pablo-CEU.

(1) Inaguma, Y.; Liquan, C.; Itoh, M.; Nakamura, T.; Uchida, T.; Ikuto, H.; Wakihara, M. *Solid State Commun.* **1993**, *86*, 689.
(2) Kawai, H.; Kuwano, J. *J. Electrochem. Soc.* **1994**, *141*, 278.
(3) Robertson, A. D.; García-Martín, S.; Coats, A.; West, A. R. *J. Mater. Chem.* **1995**, *5*, 1405.
(4) Inaguma, Y.; Chen, L.; Itoh, M.; Nakamura, T. *Solid State Ionics* **1994**, *70−71*, 196.
(5) Inaguma, Y.; Itoh, M. *Solid State Ionics* **1996**, *86−88*, 257.
(6) Harada, Y.; Ishigaki, T.; Kawai, H.; Kuwano, J. *Solid State Ionics* **1998**, *108*, 407.
(7) Brous, J.; Fankuchen, I.; Banks, E. *Acta Crystallogr.* **1953**, *6*, 67.
(8) Patil, P. V.; Chincholkar, V. S. *Curr. Sci.* **1970**, *39*, 348.
(9) Varaprasad, A. M.; Shashi, Mohan, A. L.; Chakrabarty, D. K.; Biswas, A. B. *J. Phys. C* **1979**, *12*, 465.
(10) Kochergina, L. L.; Khakhin, N. B.; Porotkinov, N. V.; Petrov, K. I. *Russ. J. Inorg. Chem.* **1984**, *29*, 879.
(11) Várez, A.; García-Alvarado, F.; Morán, E.; Alario-Franco, M. A. *J. Solid State Chem.* **1995**, *118*, 78.

space group with two different positions (1a and 1b) for the lanthanum and lithium ions along the *c*-axis. Fourquet's results have been used to try to index the powder neutron diffraction pattern of a mixture of phases in which the major phase is claimed to have the composition $La_{1.12}Li_{0.62}Ti_2O_6$.[13]

A cubic $a = 2a_p$ cell has also been considered for $La_{0.5}Li_{0.5}TiO_3$ from electron diffraction patterns,[14] and a hexagonal unit cell of lattice parameters $a = 5.47$ Å and $c = 13.4$ Å has been suggested for this oxide studied by powder neutron diffraction.[15]

More recent powder neutron diffraction studies have proposed $2a_p \times 2a_p \times 2a_p$ unit cells for $La_{0.63}Li_{0.12}TiO_3$[16] and $La_{0.62}Li_{0.15}TiO_3$[17] as being due to the tilting of the TiO_6 octahedra and ordering of the Li and La ions.

An important feature of the $La_{2/3-x}Li_{3x}TiO_3$ oxides was first reported by Robertson et al.[3] They found significant modifications of the powder X-ray diffraction patterns with the thermal treatment of the samples, proposing a phase diagram for the system. Superlattice reflections (based on a unit cell of dimensions $a_p \times a_p \times 2a_p$) weaken when increasing the annealing temperature, in such a way that the patterns of the samples annealed and quenched from the highest temperatures can be indexed as cubic perovskites. This observation and similar conclusions have been confirmed in other studies for some compositions of this solid solution.[18−20]

In addition, electron diffraction and high-resolution transmission electron microscopy studies on similar systems such as $Nd_{0.5+x}Li_{0.5-3x}TiO_3$,[21] $La_{2/3}Li_xTi_{1-x}Al_xO_3$,[22] and $La_{2/3-x}Sr_xLi_xTiO_3$[23] reveal the importance of the microstructure to be considered for determining the crystal structure of these materials. All of these titanates have similar electron diffraction patterns, which suggest a similar unit cell ($\sqrt{2}a_p \times \sqrt{2}a_p \times 2a_p$), with no dependence on either the thermal treatment of the samples or their composition.

Real crystalline solids are far from the ideal periodic arrangement of atoms (or molecules) assumed by the simplest theoretical approach to diffraction. In fact, the structure of all materials lies between the idealized crystalline and the completely disordered amorphous state. The knowledge of the real (defective) structure of a material is very important to understand how the material is built and to explain many of its properties. Solid electrolytes are, probably, one of the most evident examples of this. Because mass transport in solids is due to the existence of defects, solid ionic conductors can only exist as real solids. Despite the title materials, $La_{2/3-x}Li_{3x}TiO_3$, being among the best ionic conductors, little attention has been paid to the study of their microstructure. The effects of microstructure on the powder diffraction patterns (either X-ray or neutron data) may indeed be significant. In fact, the broadness of the superlattice reflections in the powder diffraction patterns of many of these oxides can be very pronounced as a consequence of strong microstructure effects. Interestingly, to account for these diffraction patterns, large super-cells of the basic perovskite cell are reported.[14−17] The Rietveld method requires as a starting point a model for the structure of the material and a nonstructural model to account for all of the contributions to the profile.[24] Thus, in an effort to account for the whole pattern, unrealistic or unnecessarily complex models may be developed for describing the average (ideal) structure of these materials. At this point, it must be stressed that real solids are usually very complex; it is not always easy to find few parameters to describe the microstructure of a material. This means that, to develop an adequate model, it is absolutely necessary to obtain diffraction data of as high as possible resolution and quality on very high-quality samples.

Therefore, to deal with the study of the crystal structure of the $La_{2/3-x}Li_{3x}TiO_3$ materials, a view of the whole system must be adopted and the dependence of the microstructure of the samples on the annealing temperature and composition must be considered. The materials chosen for this work have the composition $La_{0.6}Li_{0.2}TiO_3$ and $La_{0.55}Li_{0.35}TiO_3$, corresponding to the values $x = 0.07$ and $x = 0.12$, respectively. In this paper, we study the $La_{0.6}Li_{0.2}TiO_3$ oxide annealed at 1000 °C and quenched from this temperature and the $La_{0.55}Li_{0.35}TiO_3$ compound treated at two different temperatures, 800 and 1000 °C, and quenched from there.

The study of these representative oxides of the $La_{2/3-x}Li_{3x}TiO_3$ solid solution was carried out by selected area electron diffraction (SAED), high-resolution transmission electron microscopy (HRTEM), and powder synchrotron X-ray diffraction. It is shown here that the SAED and HRTEM results are indispensable for analyzing the powder synchrotron X-ray diffraction data to account for both the average structure and the microstructure of the materials.

Experimental Section

The $La_{0.6}Li_{0.2}TiO_3$ and $La_{0.55}Li_{0.35}TiO_3$ oxides were prepared from stoichiometric amounts of Li_2CO_3, La_2O_3, and TiO_2. La_2O_3 was dried overnight at 1000 °C and TiO_2 at 600 °C prior to being weighed. The mixtures were ground and heated in Pt boats, initially at 700 °C during 2 h for decarbonation. Afterward, the samples were ground, pelleted, covered with powder of the same composition to prevent lithia loss, and fired at 1100 °C for 1 day followed by a further grinding, pelleting, and firing at 1200 °C for another day to complete the reaction. After preparation, the thermal treatments were carried out with small amounts of samples which were wrapped in Pt foil envelopes, annealed isothermally at different temperatures, and quenched to room temperature on a brass plate. A sample of $La_{0.6}Li_{0.2}TiO_3$ was annealed at 1000 °C and quenched from that temperature, and two portions of $La_{0.55}Li_{0.35}TiO_3$ were annealed at 800 and 1000 °C, respectively, and quenched from there.

Crystalline phase identification was carried out by powder X-ray diffraction using a Philips X'PERT diffractometer with Cu Kα1 radiation ($\lambda = 1.5406$ Å) and with a curved Cu monochromator.

(12) Fourquet, J. L.; Duroy, H.; Crosnier-López, M. P. *J. Solid State Chem.* **1996**, *127*, 283.
(13) Ruiz, A. I.; López, M. L.; Veiga, M. L.; Pico, C. *J. Solid State Chem.* **1999**, *148*, 329.
(14) Chung, H. T.; Cheong, D. S. *Solid State Ionics* **1999**, *120*, 197.
(15) Alonso, J. A.; Sanz, J.; Santamaría, J.; León, C.; Várez, A.; Fernández-Díaz, M. T. *Angew. Chem., Int. Ed.* **2000**, *39*, 619.
(16) Sanz, J.; Alonso, J. A.; Várez, A.; Fernández-Díaz, M. T. *J. Chem. Soc., Dalton Trans.* **2002**, 1406.
(17) Inaguma, Y.; Katsumata, T.; Itoh, M.; Morii, Y. *J. Solid State Chem.* **2002**, *166*, 67.
(18) Harada, Y.; Ishigaki, T.; Kawai, H.; Kuwano, J. *Solid State Ionics* **1998**, *108*, 407.
(19) Harada, Y.; Hirasoko, Y.; Kawai, H.; Kuwano, J. *Solid State Ionics* **1999**, *121*, 245.
(20) Várez, A.; Ibarra, J.; Rivera, A.; León, C.; Santamaría, J.; Laguna, M. A.; Sanjuán, M. L.; Sanz, J. *Chem. Mater.* **2003**, *15*, 225.
(21) García-Martín, S.; García-Alvarado, F.; Robertson, A. D.; West, A. R.; Alario-Franco, M. A. *J. Solid State Chem.* **1997**, *128*, 97.
(22) Morata-Orrantia, A.; García-Martín, S.; Morán, E.; Alario-Franco, M. A. *Chem. Mater.* **2002**, *14*, 2871.
(23) Morata-Orrantia, A.; García-Martín, S.; Alario-Franco, M. A. *Chem. Mater.* **2003**, *15*, 363.
(24) *The Rietveld Method*; Young, R. A., Ed.; IUCr Monographs on Crystallography 5; Oxford University Press: Oxford, 1993.

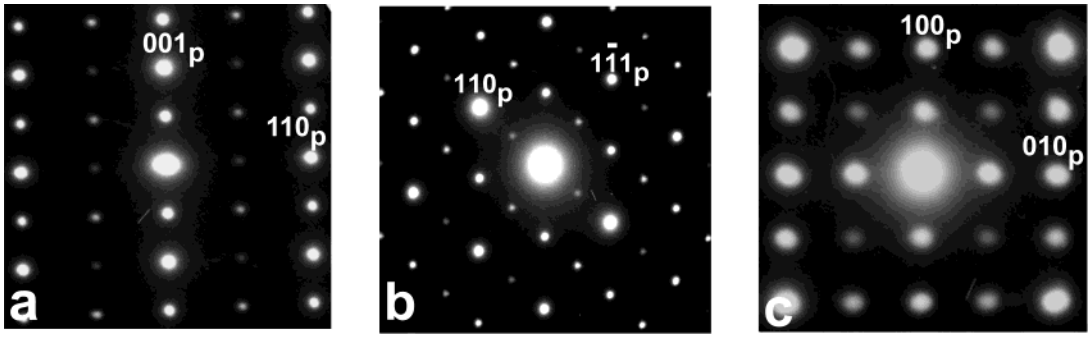

Figure 1. SAED patterns of $La_{0.55}Li_{0.35}TiO_3$ annealed at 800 °C along the (a) $[\bar{1}10]_p$, (b) $[1\ \bar{1}\ \bar{2}]_p$, and (c) $[001]_p$ zone axes.

For transmission electron microscopy, the samples were ground in *n*-butyl alcohol and ultrasonically dispersed. A few drops of the resulting suspension were deposited in a carbon-coated grid. SAED studies were performed with an electron microscope JEOL 2000FX (double tilt ±45°) working at 200 kV, and HRTEM studies were performed with an electron microscope JEOL 400 EX (double tilt ±25°) working at 400 kV.

Synchrotron X-ray diffraction (SXRD) experiments were performed on the B2 line at HasyLab using a wavelength of $\lambda = 1.252240$ Å, working in transmission and high-resolution mode as described in ref 25. In high-resolution mode, the instrumental resolution is negligible for most of the samples due to its extremely small contribution to the full-width at half-maximum (fwhm) as compared to sample effects. This contribution, measured on a suitable standard,[25] is about 0.006° for the whole 2θ-range. Concerning the peak shape, nearly Lorentzian-shaped peaks should be obtained for good samples, but, again, sample effects are predominant.

For the reasons stated in the Introduction, we have undertaken the refinement of the structures of our materials, taking into account, simultaneously, the effects of their microstructure and defects on the diffraction patterns. To handle the real structure effects in the Rietveld method, several models have been developed in detail and implemented in the programs used for structure refinement.[26] However, none of those models, based on simplified or general-purpose approaches, gave satisfactory fitting of our data. Thus, we have applied a phenomenological approach. For doing this, a new capability of the FullProf[27] program which allows some of the peaks to be described by their own breadths and shapes, as well as small displacements from their positions calculated from the average unit cell, was used. Prior to the structure refinements, a pattern matching without structural model was performed. This allows one to obtain suitable profile parameters, including the breadths, shapes, and displacements of those reflections with relevant microstructural contributions. The structural model is then refined, keeping constant the profile parameters. If needed, along the refinements some of these profile parameters are allowed to vary, but at the final steps of the refinements they are kept constant. For the structural models presented in this paper, the refinements were stable provided the number of refined parameters was low enough to obtain an adequate peaks-to-parameters ratio. To ensure this, isotropic thermal factors (ITF) are used, and all of the oxygen atoms were constrained to have the same value for ITF. The fitting process was finished when convergence was reached.

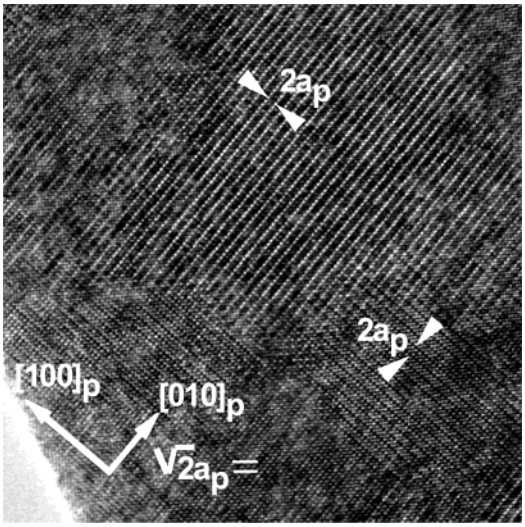

Figure 2. HRTEM image corresponding to the $[001]_p$ zone axis of $La_{0.55}Li_{0.35}TiO_3$ annealed at 800 °C.

Finally, we accomplished the study of the microstructure of these compounds by the two-step procedure proposed by Langford and Louër.[28−30]

Results and Discussion

Electron Diffraction and Microscopy. $La_{0.55}Li_{0.35}TiO_3$ Annealed at 800 °C. Figure 1 shows three different SAED patterns of this oxide in which the Bragg reflections have been indexed according to the ideal perovskite cell. The pattern corresponding to the $[\bar{1}10]_p$ zone axis (p refers to the cubic perovskite subcell) (Figure 1a) shows $(0\ 0\ l/2)_p$ superlattice reflections which double the *c* parameter of the basic cubic cell. These superlattice reflections are also observed in the conventional powder X-ray diffraction pattern (see ref 3). Moreover, $(h/2\ h/2\ l/2)_p$ reflections (not observed by XRD) can clearly be seen; $(h/2\ h/2\ 0)_p$ reflections also appear in the patterns corresponding to the $[1\ \bar{1}\ \bar{2}]_p$ and $[001]_p$ zone axes (Figure 1b and 1c). These results discard the possibility of a cell with lattice parameters $a \approx a_p$, $b \approx a_p$, $c \approx 2a_p$; thus, a new cell of dimensions $\sqrt{2}a_p \times \sqrt{2}a_p \times 2a_p$ or $2a_p \times 2a_p \times 2a_p$ must be considered. Even more, in the pattern of the $[001]_p$ zone axis,

(25) Knapp, M.; Ehrenberg, H.; Fuess, H.; Hahn, U.; Hesse, M.; Schulte-Schrepping, H.; Wroblewski, T. *Nucl. Instrum. Methods Phys. Res., Sect. A* **2001**, *467−468*, 291.
(26) Le Bail, A. In *Defect and Microstructure Analysis by Diffraction*; Snyder, P., Fiala, F., Bunge, H., Eds.; IUCr Monographs on Crystallography 10; Oxford University Press: Oxford, 1999; pp 535−555.
(27) Rodríguez-Carvajal, J. *Physica B* **1993**, *19*, 55. See also a recent report in CPD of IUCr, Newsletter 26, 12−19, 2001, available at http://www.iucr.org/iucr-top/comm/cpd/Newsletters/. The program and manual can be found at http://www-llb.cea.fr/fullweb/powder.htm.
(28) Langford, J. I. NIST Special Publication 846; Proceedings of the International Conference "Accuracy in Powder Diffraction II", Gaithersburg, MD, 1992.
(29) Langford, J. I. In *Defect and Microstructure Analysis by Diffraction*; Snyder, P., Fiala, F., Bunge, H., Eds.; IUCr Monographs on Crystallography 10; Oxford University Press: Oxford, 1999; pp 59−81.
(30) Louër, D. In *Defect and Microstructure Analysis by Diffraction*; Snyder, P., Fiala, F., Bunge, H., Eds.; IUCr Monographs on Crystallography 10; Oxford University Press: Oxford, 1999; pp 671−697.

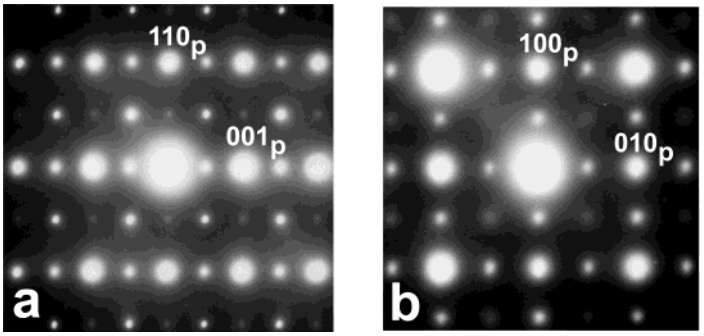

Figure 3. SAED patterns of $La_{0.55}Li_{0.35}TiO_3$ annealed at 1000 °C along the (a) $[\bar{1}10]_p$ and (b) $[1\ \bar{1}\ \bar{2}]_p$ zone axes.

reflections are observed at $(h/2\ 0\ 0)_p$ and $(0\ k/2\ 0)_p$, which double the *a*- and *b*-axes, that lead Chung et al.[14] to suggest a cell of lattice parameters $a \approx 2a_p$, $b \approx 2a_p$, $c \approx 2a_p$ for their sample.

However, the existence of crystal-domains of a $\sqrt{2}a_p \times \sqrt{2}a_p \times 2a_p$ cell with different orientations of the *c*-axis can also explain this SAED pattern (it is formed by the superposition of the patterns of the different domains).[31,32] Electron microscopy has to be used to clarify which of the two possibilities is correct. Figure 2 shows the HRTEM image corresponding to the $[001]_p$ zone axis of our material.

The crystal presents three different kinds of domains: domains with contrasting differences of $\sim 2a_p$ periodicity along $[001]_p$, domains of $\sim 2a_p$ periodicity along $[010]_p$, and domains in which an average perovskite lattice is visible but weak fringes separating a distance corresponding to $\sim\sqrt{2}a_p$ are superimposed. These fringes are situated along the $[110]_p$ direction. However, $2a_p \times 2a_p$ periodicity is not observed in the image except, of course, in the domain-boundaries, discarding then the $2a_p \times 2a_p \times 2a_p$ unit cell. Therefore, the crystal structure of the $La_{0.55}Li_{0.35}TiO_3$ oxide annealed at 800 °C is based on a perovskite-related cell with lattice parameters $a \approx \sqrt{2}a_p$, $b \approx \sqrt{2}a_p$, $c \approx 2a_p$. In addition, all of the crystals consist of domains of this cell; in each domain, the long *c*-axis is oriented along one of the three main crystallographic directions.

It should also be mentioned that splitting of the $(h\ h\ l)_p$ reflections is observed far away from the origin in the SAED patterns (the magnification of the patterns of Figure 1 does not allow the splitting to be observed). This is due to the slightly different size of the *a* and *b* lattice parameters and the domains present in the material.

$La_{0.55}Li_{0.35}TiO_3$ Annealed at 1000 °C. This material shows a conventional powder X-ray diffraction pattern (see ref 3) in which superlattice reflections of the perovskite structure have almost disappeared. However, these superlattice reflections are clearly seen on the SAED patterns. Figure 3 shows two SAED patterns of this oxide. In the pattern corresponding to the $[\bar{1}10]_p$ zone axis (Figure 3a), supperlattice $(0\ 0\ l/2)_p$ and $(h/2\ h/2\ l/2)_p$ reflections are again observed.

The $(hhl)_p$ reflections are split at high diffraction angles (not observed in Figure 3 due to insufficient magnification) as a consequence of the different sizes of the *a*- and *b*-axes and the domain formation. The pattern of the $[001]_p$ zone axis (Figure 3b) shows $(h/2\ 0\ 0)_p$ and $(0\ k/2\ 0)_p$ reflections. The HRTEM image corresponding to this last pattern (Figure 4) is characteristic of a microdomain microstructure: contrast differences with periodicity $\sim 2a_p$ are observed in different parts of the crystal along both the $[100]_p$ and the $[010]_p$ directions, while lattice fringes at $\sim\sqrt{2}a_p$ distances are also seen along the $[110]_p$ direction. This means that, once again, microdomains with the long $\sim 2a_p$-axis oriented along the three space directions are randomly distributed over the crystal.

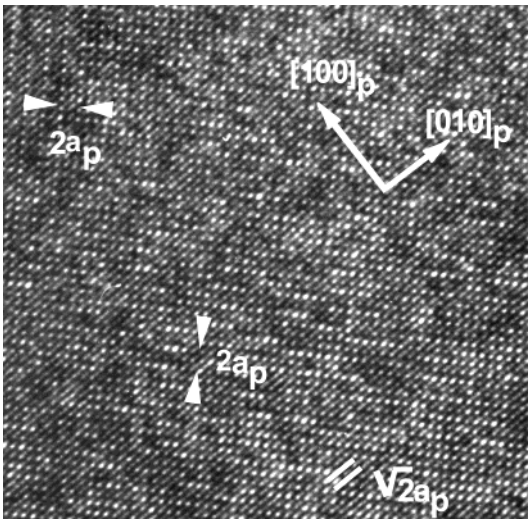

Figure 4. HRTEM image corresponding to the $[001]_p$ zone axis of $La_{0.55}Li_{0.35}TiO_3$ annealed at 1000 °C.

Therefore, the $La_{0.55}Li_{0.35}TiO_3$ material, annealed at 1000 °C and quenched from this temperature, has the same basic unit cell ($\sim\sqrt{2}a_p \times \sim\sqrt{2}a_p \times \sim 2a_p$) as the compound kept at 800 °C, despite the differences observed in their powder X-ray diffraction patterns. The microstructure of the material changes with the thermal treatment, and the size of the diffracting domains decreases with an increase in the annealing temperature. In fact, the domain size seems to correspond to just a few unit cells when the sample is annealed at 1000 °C (Figure 4).

$La_{0.6}Li_{0.2}TiO_3$ Annealed at 1000 °C. The powder X-ray diffraction pattern of this material is similar to that of the sample $La_{0.55}Li_{0.35}TiO_3$ annealed at 800 °C and quenched afterward (i.e., superlattice reflections of the perovskite structure appear). This kind of pattern is observed over a wide range of annealing temperatures, and only above 1200 °C does it seem to turn into a cubic perovskite cell.[3]

Figure 5 shows different SAED patterns of this oxide. As expected, in the pattern of the $[\bar{1}\ 1\ 0]_p$ zone axis (Figure 5a), superlattice reflections $(0\ 0\ l/2)_p$ and $(h/2\ k/2\ l/2)_p$ are seen, the latter being clearly split into two at high diffraction angles (see arrows in Figure 5a).

(31) Alario-Franco, M. A.; Joubert, J. C.; Lévy, J. P. *Mater. Res. Bull.* **1982**, *17*, 733.
(32) Vegas, A.; Vallet-Regí, M.; González-Calbet, J. M.; Alario-Franco, M. A. *Acta Crystallogr., Sect. B* **1986**, *42*, 167.

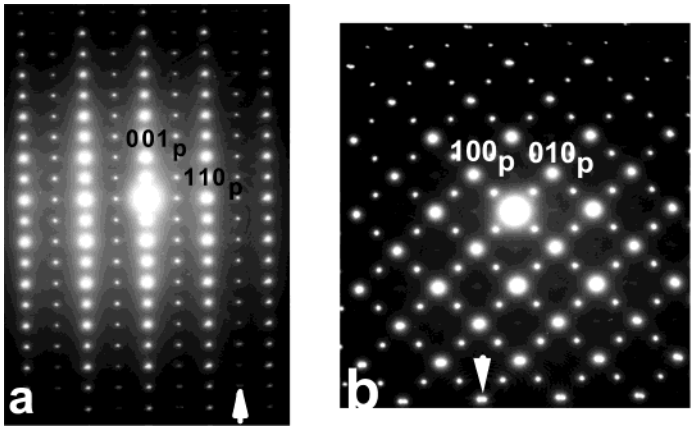

Figure 5. SAED patterns of $La_{0.60}Li_{0.20}TiO_3$ annealed at 1000 °C along the (a) $[\bar{1}10]_p$ and (b) $[1\ \bar{1}\ \bar{2}]_p$ zone axes.

The patterns corresponding to the $[0\ 0\ 1]_p$ zone axis (Figure 5b) show $(h/2\ 0\ 0)_p$, $(0\ k/2\ 0)_p$, and $(h/2\ k/2\ 0)_p$ reflections. The $(h/2\ k/2\ 0)_p$ reflections are weak, and, due to the splitting, they look like rows instead of regular spots. These reflections are split into four in some of the $Nd_{0.5+x}Li_{0.5-3x}TiO_3$ ($0.016 < x < 0.12$) and $La_{1/3-x}Li_{3x}NbO_3$ ($0 \leq x \leq 0.06$) oxides and in $ThNb_4O_{12}$.[21,33,34] This splitting is due to the existence of a microdomain microstructure in which the system of the tilting of the BO_6 octahedra (B = Ti, Nb) is twinned.

In addition to this, the main perovskite reflections in the pattern of the $[0\ 0\ 1]_p$ zone axis are also split into two (see arrows in Figure 5b). This is a consequence of the domain-microstructure and the different size of the $a \approx \sqrt{2}a_p$ and $b \approx \sqrt{2}a_p$ lattice parameters.

The HRTEM images corresponding to the $[0\ 0\ 1]_p$ zone axis of this oxide also show domains with different orientations of the long $\sim 2a_p$-axes. As in $La_{0.55}Li_{0.35}TiO_3$ annealed at 800 °C (Figure 2), the domains are large enough to allow the $(0\ 0\ 1/2)_p$ reflection to be well observed by powder X-ray diffraction, although they are still broader than the reflections associated with the basic unit cell. These results indicate that the $La_{0.6}Li_{0.2}TiO_3$ material annealed at 1000 °C and quenched from that temperature also has basic unit cell parameters $a \approx \sqrt{2}a_p$, $b \approx \sqrt{2}a_p$, $c \approx 2a_p$.

The diagonal unit cell seems then to be common for all of the oxides of the system with no dependence on the composition or on the annealing temperature. We can now propose a structural model based on this cell. Tilting of the BO_6 octahedra is the most common distortion of the ABO_3 simple perovskites. In addition to this, ordering of the La and Li ions within the A-sites seems to occur in our materials; $(0\ 0\ l/2)_p$ $l = 2n + 1$ reflections are related to this ordering. All of these features will be used to develop a suitable structural model for these oxides. The results of the refinement of the average (ideal) structure and the real structure (microstructure) will be presented in the next subsections.

Synchrotron Powder X-ray Diffraction. Crystal Structure Refinement. Figures 6−8 show the graphic result of the fitting of the experimental high-resolution synchrotron X-ray diffraction patterns corresponding to $La_{0.60}Li_{0.2}TiO_3$ quenched from 1000 °C, $La_{0.55}Li_{0.35}TiO_3$ quenched from 800 °C, and $La_{0.55}Li_{0.35}TiO_3$ quenched from 1000 °C, respectively, as well as the differences between the observed and the calculated data. In the inset, details of two regions of the patterns are shown enlarged.

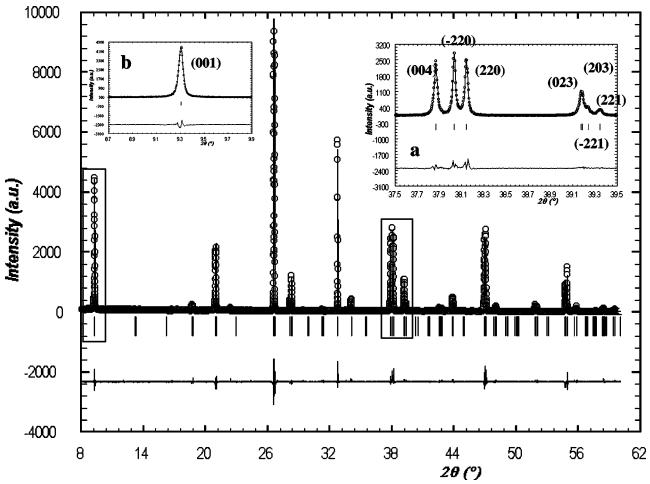

Figure 6. Experimental (points), calculated (solid line), and difference (bottom) synchrotron X-ray diffraction patterns for $La_{0.60}Li_{0.2}TiO_3$ quenched from 1000 °C. (a) Magnification of a zone of the pattern to show monoclinic symmetry of the structure (see text). (b) Fitting of the (001) peak; the microstructure effects are evident.

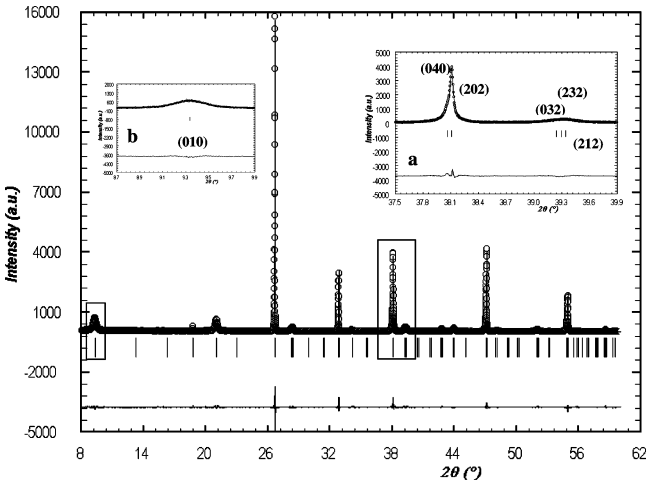

Figure 7. Experimental (points), calculated (solid line), and difference (bottom) synchrotron X-ray diffraction patterns for $La_{0.55}Li_{0.35}TiO_3$ quenched from 800 °C. (a) Magnification of a zone of the pattern to show the orthorhombic symmetry of the material (see text). (b) Fitting of the (010) peak; the microstructure effects are evident.

(33) García-Martín, S.; Alario-Franco, M. A. *J. Solid State Chem.* **1999**, *148*, 93.

Table 1. Structure Parameters of $La_{2/3-x}Li_{3x}TiO_3$ as Refined from Synchrotron X-ray Diffraction Data

		$La_{0.55}Li_{0.35}TiO_3$ quenched from 1000 °C[a]					$La_{0.55}Li_{0.35}TiO_3$ quenched from 800 °C[b]				
atom	site[d]	*x/a*	*y/b*	*z/c*	B_{iso} (A^2)	occ.[f]	site[d]	*x/a*	*y/b*	*z/c*	B_{iso} (A^2)	occ.[f]
La(1)	2e	1/4	0	0.751(3)	0.38(6)	0.140(2)	2e	1/4	0	0.760(2)	0.42(3)	0.05(1)
La(2)	2f	3/4	1/2	0.246(2)	0.40(6)	0.163(2)	2f	3/4	1/2	0.2530(3)	0.41(3)	0.24(1)
Ti	4k	1/4	0.2492(9)	0.2502(3)	0.01(4)	1/2	4k	1/4	0.2446(2)	0.2500(5)	0.07(4)	1/2
O(1)	2e	1/4	0	0.229(9)	0.6(1)	1/4	2e	1/4	0	0.288(2)	0.50(7)	1/4
O(2)	4g	0	0.265(3)	0	0.6(1)	1/2	4g	0	0.271(1)	0	0.50(7)	1/2
O(3)	2f	3/4	1/2	0.712(8)	0.6(1)	1/4	2f	3/4	1/2	0.721(2)	0.50(7)	1/4
O(4)	4h	1/2	0.763(3)	1/2	0.6(1)	1/2	4h	1/2	0.751(1)	1/2	0.50(7)	1/2

		$La_{0.60}Li_{0.20}TiO_3$ quenched from 1000°C[c]				
atom	site[e]	*x/a*	*y/b*	*z/c*	B_{iso} (A^2)	occ.[f]
La(1)	2m	0.2492(5)	0.7520(5)	0	0.73(3)	1/2
La(2)/Li	2n	0.754(2)	0.229(2)	1/2	0.74(3)	0.12(2)/0.18(2)
Ti	4o	0.252(2)	0.2506(9)	0.2640(2)	0.69(5)	1
O(1)	2m	0.290(3)	0.265(3)	0	0.46(8)	1/2
O(2)	2n	0.215(3)	0.227(4)	1/2	0.46(8)	1/2
O(3)	2i	0	0	0.233(2)	0.46(8)	1/2
O(4)	2k	1/2	0	0.232(4)	0.46(8)	1/2
O(5)	2l	1/2	1/2	0.261(1)	0.46(8)	1/2
O(6)	2j	0	1/2	0.226(4)	0.46(8)	1/2

[a] $a = 5.4353(1)$ Å, $b = 7.6942(1)$ Å, $c = 5.4366(1)$ Å, $V = 227.36(1)$ Å^3, $R_B = 0.040$, $R_W = 0.16$, $R_{exp} = 0.12$, $\chi^2 = 1.66$. [b] $a = 5.4276(1)$ Å, $b = 7.6947(1)$ Å, $c = 5.4126(1)$ Å, $V = 226.05(1)$ Å^3, $R_B = 0.044$, $R_W = 0.135$, $R_{exp} = 0.10$, $\chi^2 = 1.74$. [c] $a = 5.4311(1)$ Å, $b = 5.4279(1)$ Å, $c = 7.7216(1)$ Å, $\gamma = 90.157(1)°$, $V = 227.63(1)$ Å^3, $R_B = 0.049$, $R_W = 0.154$, $R_{exp} = 0.098$, $\chi^2 = 2.48$. [d] Space group = *Pmma* (No. 51). [e] Space group = *P*..2/*m* (No. 10). [f] Occupation given as multiplicity of the site divided by multiplicity of the space group.

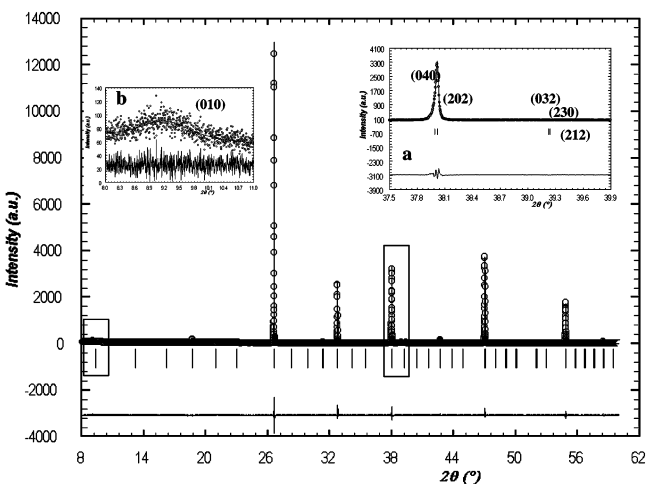

Figure 8. Experimental (points), calculated (solid line), and difference (bottom) synchrotron X-ray diffraction patterns for $La_{0.55}Li_{0.35}TiO_3$ quenched from 1000 °C. (a) Magnification of a zone of the pattern to show the orthorhombic symmetry (see text). (b) Fitting of the (010) peak; strong microstructure effects are evident.

The calculated patterns were obtained using the final structural parameters collected in Table 1, whereas Table 2 shows some selected structural information.

The starting structural model was developed from the results given by SAED and HREM described above and from crystallographic studies of perovkites.[35−43] Thus, the unit cell for the three samples is assumed to be a so-called diagonal cell: $\sqrt{2}a_p \times \sqrt{2}a_p \times 2a_p$.

Because no extinctions are observed, the apparent symmetry corresponds to the space group *Pmmm*. It is well established that superstructures in perovskites can be produced by two main mechanisms: tilting of the ocatehdra and cation ordering in either the B- or the A-sites (or both) of the perovskite structure.[35−43]

In simple perovskites (i.e., with one type of A and B ions), Howard et al.[42] predicted the unit cell parameters and the symmetry by a group theoretical analysis of the possible octahedra tilting schemes. Interestingly, only four systems ($a^0a^0c^-$, $a^0b^-b^-$, $a^+b^-b^-$, and $a^+b^-c^-$ in Glazer's notation,[35,36] corresponding to space groups *I*4/*mcm*, *Imma*, *Pnma*, and $P2_1/m$, respectively) yield a diagonal unit cell.[40−42] The tetragonal group and any tetragonal subgroup of it can be discarded because our materials are undoubtedly orthorhombic (or monoclinic). This is clear from the splitting of the main Bragg reflections on the SAED patterns.

On the other hand, $La_{2/3-x}Li_{3x}TiO_3$ materials are not simple perovskites. The ordering of lanthanum, lithium, and vacancies eliminates the I-centering associated with the $a^0b^-b^-$ tilting system and is not compatible with the screw axis associated with the tilting scheme $a^+b^-c^-$. When the ordering is considered for the $a^+b^-b^-$ tilting system, the resulting symmetry is $P2_1ma$ (keeping the cell orientation as $\sqrt{2}a_p \times 2a_p \times \sqrt{2}a_p$). This space group, as well as the *Pmma* symmetry resulting from the ordering in the $a^0b^-b^-$ tilting system, are compatible with our SAED patterns; the extinctions due to the *a*-glide plane and the screw axis are not observed due to the domain microstructure of these materials. Finally, the orthorhombic subgroups of the tetragonal *I*4/*mcm* group are neither compatible with the SAED patterns and HRTEM images (*Pcna* and *Pcma*), nor with the diagonal cell (*Cmma* and *Cmmm*). Thus, the symmetry to be expected in these materials, according to the theoretical predictions[35−42] and supported by our results, would be orthorhombic *Pmma* (No. 51) or its acentric subgroup $P2_1ma$ (No.

(34) Alario-Franco, M. A.; Grey, I. E.; Joubert, J. C.; Vincent, H.; Labeau, M. *Acta Crystallogr., Sect. A* **1982**, *38*, 177.
(35) Glazer, A. M. *Acta Crystallogr., Sect. B* **1972**, *28*, 3384.
(36) Glazer, A. M. *Acta Crystallogr., Sect. A* **1975**, *31*, 756.
(37) O'Keefe, M.; Hyde, B. G. *Acta Crystallogr., Sect. B* **1977**, *33*, 3802.
(38) Thomas, N. W. *Acta Crystallogr., Sect. B* **1989**, *45*, 337.
(39) Thomas, N. W. *Acta Crystallogr., Sect. B* **1996**, *52*, 16.
(40) Woodward, P. M. *Acta Crystallogr., Sect. B* **1997**, *53*, 32.
(41) Woodward, P. M. *Acta Crystallogr., Sect. B* **1997**, *53*, 44.
(42) Howard, C. J.; Stokes, H. T. *Acta Crystallogr., Sect. B* **1998**, *54*, 782.
(43) Bock, O.; Müller, U. *Acta Crystallogr., Sect. B* **2002**, *58*, 594−606.

Table 2. Selected Structural Information for $La_{2/3-x}Li_{3x}TiO_3$ (Distances up to 3.00 Å)

$La_{0.55}Li_{0.35}TiO_3$ quenched from 1000 °C		$La_{0.55}Li_{0.35}TiO_3$ quenched from 800 °C		$La_{0.6}Li_{0.2}TiO_3$ quenched from 1000 °C	
Ti−O(1)	1.921(8)	Ti−O(1)	1.894(2)	Ti−O(1)	2.049(3)
Ti−O(2)	1.93(1) × 2	Ti−O(2)	1.927(2) × 2	Ti−O(2)	1.852(4)
Ti−O(3)	1.941(8)	Ti−O(3)	1.971(2)	Ti−O(3)	1.96(1)
Ti−O(4)	1.92(1) × 2	Ti−O(4)	1.916(2) × 2	Ti−O(4)	1.92(1)
average	1.927(4)	average	1.925(1)	Ti−O(5)	1.90(1)
distortion[a]	0.11×10^{-4}	distortion[a]	1.48×10^{-4}	Ti−O(6)	1.96(1)
				average	1.938(4)
La(1)−O(1)	2.84(6)	La(1)−O(1)	2.55(1)	distortion[a]	10.11×10^{-4}
La(1)−O(1)^{i}	2.60(5)	La(1)−O(1)^{i}	2.86(1)		
La(1)−O(1)^{ii}	2.720(2) × 2	La(1)−O(1)^{ii}	2.726(1) × 2	La(1)−O(1)	2.60(2)
La(1)−O(2)	2.80(2) × 4	La(1)−O(2)	2.807(2) × 4	La(1)−O(1)^{i}	2.84(2)
La(1)−O(4)	2.65(2) × 4	La(1)−O(4)	2.736(7) × 4	La(1)−O(1)^{ii}	2.90(2)
site potential (eV)	−11.2	site potential (eV)	−9.0	La(1)−O(1)^{iii}	2.54(2)
				La(1)−O(3)	2.611(9) × 2
La(2)−O(2)	2.63(2) × 4	La(2)−O(2)	2.611(6) × 4	La(1)−O(4)	2.64(3) × 2
La(2)−O(3)	2.90(4)	La(2)−O(3)	2.88(1)	La(1)−O(5)	2.801(9) × 2
La(2)−O(3)^{i}	2.53(4)	La(2)−O(3)^{i}	2.53(1)	La(1)−O(6)	2.61(3) × 2
La(2)−O(3)^{ii}	2.727(4) × 2	La(2)−O(3)^{ii}	2.717(1) × 2	site potential (eV)	−15.7
La(2)−O(4)	2.80(2) × 4	La(2)−O(4)	2.714(6) × 4		
site potential (eV)	−11.8	site potential (eV)	−14.1	La(2)/Li−O(2)	2.42(2)
				La(2)/Li −O(2)^{i}	2.46(2)
				La(2)/Li −O(2)^{ii}	2.99(2)
				La(2)/Li−O(3)	2.76(1) × 2
				La(2)/Li−O(4)	2.76(3) × 2
				La(2)/Li−O(5)	2.74(1) × 2
				La(2)/Li−O(6)	2.89(3) × 2
				site potential (eV)	−7.5

[a] Distortion $= 1/n\sum[(d_i - \langle d\rangle)/\langle d\rangle]^2$.

26), or monoclinic $P2/m$ (No. 10, unique axis b). For all of these groups, the unit cell orientation is $\sqrt{2}a_p \times 2a_p \times \sqrt{2}a_p$.

From Figures 6a, 7a, and 8a (see reflections about 38°(2θ)), it is evident that the only material of monoclinic symmetry is that of composition $La_{0.60}Li_{0.2}TiO_3$ quenched from 1000 °C, the other two samples being of higher symmetry (orthorhombic). Therefore, to fit the data corresponding to the samples of composition $La_{0.55}Li_{0.35}TiO_3$, we tried structural models of *Pmma* and $P2_1ma$ symmetries. Despite that the latter model had more parameters, the refinement did not improve and became unstable. Thus, *Pmma* symmetry was preferred.

The crystal structures of the three compounds are similar (Figure 9 and Supporting Information); despite the different symmetry, they have some common features. The formation of a superstructure of the basic perovskite is due to two mechanisms in the three cases: the tilting of octahedra and the ordering of La^{3+}, Li^{+}, and vacancies in the A-site of the perovskite along the $2a_p$-axis.

Interestingly, the tilting system seems to be the same in the three materials: $a^0b^-b^-$. However, as deduced from the refined parameters collected in Table 1, the tilting system is strictly so only in $La_{0.55}Li_{0.35}TiO_3$ quenched from 1000 °C (Supporting Information). In the other two cases, the TiO_6 octahedra are so distorted that some oxygen atoms do not obey the tilting scheme (Figure 9 and Supporting Information). It must be recalled that the tilting schemes in references 35−42 are derived for rigid BO_6 octahedra, and, as pointed out by Howard,[42] in most cases there is no reason for the octahedra to be rigid. This is especially right in complex perovkites such as $La_{2/3-x}Li_{3x}TiO_3$ in which the A-sites are shared by ions of very different size such as La^{3+} and Li^{+}[44] and vacancies. Thus, the TiO_6 octahedra are distorted (see Table 2) to accommodate the small lithium ions and the vacancies. In fact, in the lanthanum-rich compound,

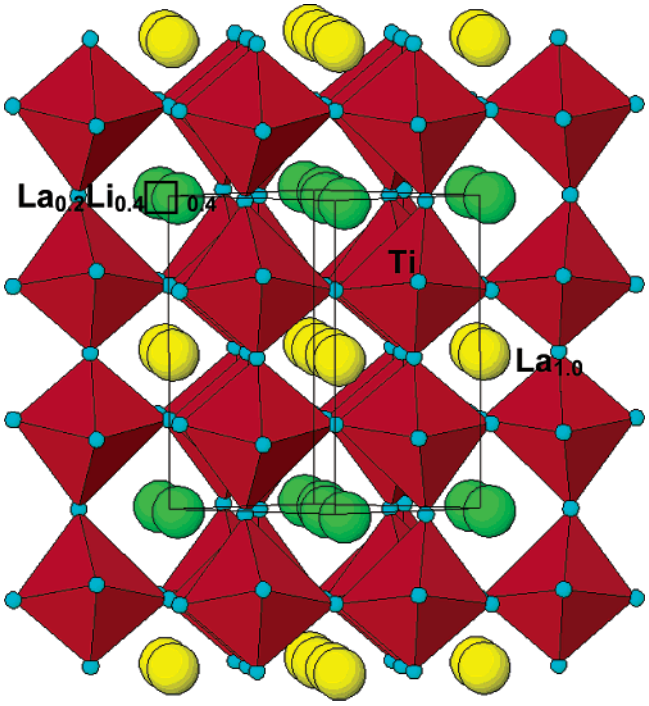

Figure 9. Schematic representation of the structure of $La_{0.60}Li_{0.20}TiO_3$ quenched from 1000 °C.

$La_{0.60}Li_{0.2}TiO_3$, the lowering in symmetry, from orthorhombic *Pmma* to monoclinic $P2/m$, seems to be most likely due to the severe distortion of the TiO_6 octahedra.

Concerning the ordering of lanthanum, lithium, and vacancies along the doubled axis ($2a_p$), as it would be expected, the degree of ordering depends on both the annealing temperature and the composition (mainly the concentration of vacancies).

Thus, in the material with 20% of vacancies in the A-site ($La_{0.60}Li_{0.20}TiO_3$) quenched from 1000 °C, lanthanum-rich layers

(44) Shannon, R. D. *Acta Crystallogr., Sect. A* **1976**, *32*, 751.

(La(1)) alternate with vacancy-rich layers (La(2)) along the $2a_p$-axis (Table 1, Figure 9). On the other hand, in the oxide with 10% of vacancies ($La_{0.55}Li_{0.35}TiO_3$) also quenched from 1000 °C, there is an almost complete disorder of vacancies, lanthanum, and lithium into the two A-sites in the structure (Table 1 and Supporting Information). However, the occupations of the two A-sites are slightly different, otherwise the $(0\ 0\ l/2)_p$ reflections with $l = 2n + 1$ should have disappeared from the SAED patterns (Figure 3a).

As stated above, the temperature of annealing also modifies the A-site ordering. When $La_{0.55}Li_{0.35}TiO_3$ is treated at lower temperature (800 °C), the degree of ordering is similar to that found in $La_{0.60}Li_{0.20}TiO_3$ with a higher concentration of vacancies. Therefore, the materials with a low concentration of vacancies ($0.1 < x < 0.14$ in $La_{2/3-x}Li_{3x}TiO_3$)[3] need to be annealed at temperatures lower than the synthesis temperature to promote ordering of lanthanum, lithium, and vacancies. Yet, the annealing temperature must be high enough to allow ions to move and to order, but not too high to promote disorder: 800 °C seems to be the most favorable temperature.[3] On the contrary, the compounds with a high concentration of vacancies ($0.04 < x < 0.10$) are ordered over a wider range of temperatures.[3]

In connection with the ordering within the A-site of the structure, it is worth pointing out that titanium ions are displaced from the center of the TiO_6 octahedra toward the vacancy-rich layers in the structure. In fact, in $La_{0.60}Li_{0.2}TiO_3$ quenched from 1000 °C and $La_{0.55}Li_{0.35}TiO_3$ quenched from 800 °C, in which La-rich and vacancy-rich layers alternate along the $2a_p$-axis, titanium is displaced by a similar length (about 0.03 Å). On the contrary, in $La_{0.55}Li_{0.35}TiO_3$ quenched from 1000 °C, the shift is only about 0.005 Å, which is within the experimental error.

A measure of the tendency of La^{3+} and Li^+ to ordering is given in Table 2 as the Madelung potential in the A-sites of the perovskite structure: the larger the difference between the two A-sites, the stronger the driving force for ordering. The La^{3+} ions tend to preferentially occupy the sites with higher negative potential, yielding an extra stabilization of the structure. Thus, in the material $La_{0.60}Li_{0.20}TiO_3$ quenched from 1000 °C, the difference of the electrostatic potential in both A-sites is so important that the La(1) site is fully occupied by lanthanum whereas the other A-site is shared by La^{3+}, Li^+, and vacancies (Table 1). As a result, La-rich and vacancy-rich layers alternate along the $2a_p$-axis. If the driving force for ordering is less pronounced, but still important, as in $La_{0.55}Li_{0.35}TiO_3$ quenched from 800 °C, some lithium (or vacancies) may occupy the most favorable position (La(2) in Tables 1 and 2). The loss of electrostatic energy must be compensated by the entropic contribution, which could be important at the treatment temperature. Finally, in $La_{0.55}Li_{0.35}TiO_3$ quenched from 1000 °C, in both A-sites the Madelung potential has almost the same value (Table 2); as a result, the occupancy of La(1) and La(2) (Table 1) is similar.

Microstructure Study. Microstructure effects are numerous and usually appear superposed; thus, the analysis of diffraction patterns to extract the real structure features is not simple. In fact, the real structure can be very complex. Parts (domains) of different size and shape and different orientations may be present; these domains may contain structural "mistakes" such as stacking faults and compositional fluctuations. Inclusions and precipitates are frequent as much as stress and strain. Each of these real-structure features has its effect on the diffraction pattern. The limited size of the domains, the presence of strain, and stacking faults, as a result, cause the broadening of the peaks; in addition, structure mistakes, such as the variation of composition along the structure and stacking faults, can also induce the displacement and asymmetry of some peaks.[29,45] Thus, in some cases, a detailed and accurate description of real structures would require a large number of parameters.

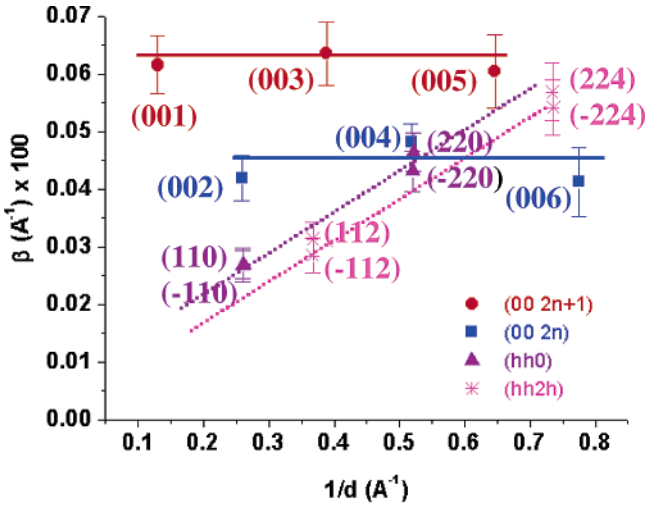

Figure 10. Williamson−Hall plot corresponding to $La_{0.60}Li_{0.20}TiO_3$ quenched from 1000 °C. Lines are guides for the eyes.

As it will be shown, $La_{2/3-x}Li_{3x}TiO_3$ materials have a complex microstructure that cannot be accounted for by the conventional models. To study the microstructure of these compounds, we have used the two-step procedure proposed by Langford.[28,29] Each peak was fitted to a pseudo-Voight function, and the integral breadths ($\beta = A/I_0$, A = integrated intensity, I_0 = maximum of intensity) and the shape parameters (ϕ = fwhm/β) were determined. The latter were checked to be within the theoretical limits for the Lorentzian ($\phi = 0.6366$) and Gaussian ($\phi = 0.9394$) functions from which the pseudo-Voigt function is built; this ensures the method can be properly applied.

Figure 10 shows the Williamson−Hall plot[46] corresponding to the sample $La_{0.60}Li_{0.2}TiO_3$ quenched from 1000 °C. The integral breadth of reflections with Miller indices (00l) (the c-axis being the $2a_p$ one) is independent of the order; that is, it is d^*-independent. This indicates that, in this direction, there is no measurable contribution of microstrains or other kinds of "lattice distortions".[29] On the contrary, the (hh0) and ($hh2h$) reflections show a clear dependence on d^*. This suggests that along the [110] direction the material would present microstrains. According to Langford[28] and Halder and Wagner,[47] the contributions to the integral breadth of strains and domain size can be separated using eq 1:

$$(\beta/d^*)^2 = \epsilon^{-1}\beta/(d^*)^2 + (\eta/2)^2 \qquad (1)$$

where ϵ gives the mean apparent domain size, and η is a measure of the strain related to the root-mean-square strain (e_{rms}) by e_{rms}

(45) Warren, B. E. *X-ray Diffraction*; Dover Publications Inc.: New York, 1990.
(46) Williamson, G. K.; Hall, W. H. *Acta Met.* **1953**, *1*, 22−31.
(47) Halder, N. C.; Wagner, C. N. J. *Adv. X-Ray Anal.* **1966**, *9*, 91−102.

$\approx \eta/5$.[29] The values obtained for ($hh0$) reflections are $\epsilon = 7000$-(900) Å, $\eta = 14(1) \times 10^{-3}$, and $e_{rms} = 2.8(2) \times 10^{-3}$.

On the other hand, it is evident from Figures 6 and 10 that (00l) reflections show different broadening as a function of the parity of l. The (00l) reflections with $l = 2n + 1$ are broader than those with even values of l. As will be shown, in this latter case, the breadths can be assigned only to domain size contributions. With this hypothesis, and assuming that the peak function is mainly Lorentzian as the values of the shape parameter suggest, the average value of the integral breadth for (0 0 2n) peaks results: $\beta_{(002n)} = 0.044(2)$ Å^{-1}. On this basis, the domain size along the c-axis can be estimated as $\langle D \rangle_{[001]} = 2300(100)$ Å. The extra breadth of l-even (00l) reflections ($\beta_{(002n+1)} = 0.062(3)$ Å^{-1}) may be due to the presence of structural mistakes along the c-axis.

There are several different kinds of structure mistakes that contribute to peak breadth. Bearing in mind the structure of these materials (Figure 9 and Supporting Information), it is easy to propose a mechanism for these structure mistakes. They are most likely due to compositional fluctuations of the A-sites layers along the $2a_p$-axis. This kind of mistake broadens the (0 0 2n+1) peaks and may produce their shifts with respect to the positions determined from the unit cell, as observed in our patterns.[29,45] Because in $La_{0.60}Li_{0.2}TiO_3$, layers of lanthanum alternate with layers of average composition $La_{0.2}Li_{0.4}\square_{0.4}$ (Table 1, Figure 9), the compositional fluctuations should occur between couples of these different layers.

To extract the microstructure information from the diffraction patterns, the formalism proposed by Wilson[48,49] was applied to the above-presented model of structural mistakes. The structure factor of a (hkl) reflection for a well-ordered cell, that is, a cell with the site occupations in Table 1, is given by $F_{(hkl)}$, in particular, for (00l) reflections and considering only the contribution of A-site ions:

$$F_{(002n)} \approx f_{La(1)} \exp(0) + f_{La(2)} \exp(2\pi n i) = f_{La(1)} + f_{La(2)} \quad (2)$$

$$F_{(002n+1)} \approx f_{La(1)} \exp(0) + f_{La(2)} \exp((2n+1)\pi i) = f_{La(1)} - f_{La(2)} \quad (3)$$

Now, the structure factor for a "defective" unit cell in which occ(La′(1)) = occ(La(1)) − Δ and occ(La′(2)) = occ(La(2)) + Δ is given by:

$$F_{(002n)}' \approx f_{La(1)} - f_{\Delta} + f_{La(2)} + f_{\Delta} = F_{(002n)} \quad (4)$$

$$F_{(002n+1)}' = f_{La(1)} - f_{\Delta} - f_{La(2)} - f_{\Delta} = f_{La(1)} - f_{La(2)} - 2f_{\Delta} = \delta F_{(002n+1)} \qquad \delta \leq 1 \quad (5)$$

Therefore, because the intensities of the (00l) $l = 2n$ reflections depend on the addition of scattering factors of La(1) and La(2), small variations of the composition of the A-sites layers have no effect either on their intensities or on their integral breadths. On the contrary, small variations of the occupancies of the A-sites (Δ) have significant relative effects on the intensities and breadths of (00l) $l = 2n + 1$ reflections.

Assuming that the size and mistake profiles are both Lorentzian (supported by the values of the shape parameter ϕ), the total breadth of (00l) $l = 2n + 1$ reflections can be expressed as:

$$\beta_{(002n+1)} = \beta_{(002n+1)}{}^{S} + \beta_{(002n+1)}{}^{m} \quad (6)$$

where $\beta_{(002n+1)}{}^{S}$ and $\beta_{(002n+1)}{}^{m}$ are the contributions due to domain size effects and structural mistakes, respectively. Because the (00l) $l = 2n$ reflections are not affected by compositional fluctuations, $\beta_{(002n+1)}{}^{S}$ can be supposed to be equal to $\beta_{(002n)}{}^{S} = 0.044(2)$ Å^{-1}; thus, $\beta_{(002n+1)}{}^{m} = 0.062(1) - 0.044(2) = 0.018(1)$ Å^{-1}.

To obtain a complete picture of the microstructure of this material, the frequency of the structural mistakes must to be determined. Let α be the probability of such a mistake to occur along the $2a_p$-axis. Equation 7, obtained using the Wilson's formalism[48] applied to this particular case, gives the dependence of the breadths of (0 0 l) l = odd with both α and the degree of local disorder between two neighboring layers, which is related to δ through eq 5.

$$\beta_{(002n+1)}{}^{m} = 9\alpha/[4(1-\delta)] \quad (7)$$

Interestingly, the δ parameter is related to the intensity of a (0 0 l) reflection with $l = 2n + 1$ in such a way that the weaker is the reflection, the lower is the value of δ.

An additional difficulty appears with eq 7 because it is not possible, with the present data, to separate the effect of the frequency of mistakes from that of the degree of disorder. Therefore, only rough estimations can be performed if some assumptions are accepted. The low value of $\beta_{(002n+1)}{}^{m}$ (0.018(1) Å^{-1}) and the relatively high intensity of the (00l) reflections with l = odd (see Figure 6b and eqs 3 and 5) suggest that the composition of A-site layers is very close to the average values in Table 1 and fluctuations from those values are seldom.

To summarize, the microstructure of $La_{0.60}Li_{0.2}TiO_3$ quenched from 1000 °C is composed of domains of lamellar shape with a basal plane of about (7000 × 7000) Å^2 on the {110} planes and a height of around 2300 Å along the $2a_p$-axis (c-axis). Also, subtle compositional fluctuations occur along the c-axis in a few A-site layers within each domain. Finally, the misfit between the (110) spacing and the (001) spacing (they differ by 0.5%) induces some strain in the {hh0} planes, and probably also in the (00l) planes, but in this case other microstructural effects are dominant.

In the Williamson−Hall plot[45] corresponding to the sample $La_{0.55}Li_{0.35}TiO_3$ quenched from 800 °C (Supporting Information), the integral breadths of all peaks seem to be d*-independent and equal for all reflections except for (0k0) k = odd (the b-axis being the $2a_p$ one).

This suggests that size effects dominate the microstructure in all directions but the b-axis. Even more, the domains can be thought of as being "spherical" or more likely of cubic shape. The average length of the cube edge is estimated to be $\langle D \rangle = 2500(100)$ Å from the average integral breadth $\beta_{(hkl)} = 0.039(4)$ Å^{-1}. Although there is no measurable contribution of microstrains on the {h0h} planes, because the b-axis and the {101} spacings differ by 0.38%, strains probably would be present in the {h0h} planes and most likely also in the (0l0) planes.

(48) Wilson, A. J. C. *X-Ray Optics*; Methuen's Monographs on Physical Subjects; Methuen and Co. Ltd.: London, 1962.
(49) Wilson, A. J. C. *Mathematical Theory of X-ray Powder Diffractometry*; Philips Technical Library: Eindhoven, Holland, 1963.

In addition to the domain-size effects, the effect of composition fluctuations is evident in this sample (Supporting Information). The breadth due to structural mistakes can be estimated as: $\beta_{(02n+10)}^{m} = \beta_{(02n+10)} - \beta_{(hkl)} = 0.381(4) - 0.039(4) = 0.342(3)$ Å^{-1}. If one assumes a degree of compositional fluctuation similar to that in the previous sample, eq 7 yields a frequency of mistakes, such as that, within the domains, every few hundreds of A-site layers a mistake occurs.

Finally, for sample $La_{0.55}Li_{0.35}TiO_3$ quenched from 1000 °C, the presence of very broad peaks and a severe peak overlapping (Figure 8) preclude a detailed microstructure analysis. Only estimations of the average size of the diffracting domains assumed to be of cubic shape, and some information about the structural mistakes (from the breadth of the (010) reflection, the only (0k0) $k = 2n + 1$ reflection that could be properly fitted), were obtained. Thus, the length of the cubic domain seems to be about $\langle D \rangle = 230(30)$ Å as obtained from the integral breadth $\beta_{(hkl)} = 0.43(6)$ Å^{-1}. Using this value and $\beta_{(010)} = 1.2(3)$ Å^{-1}, the breadth due to structure mistakes can be estimated to be: $\beta_{(02n+10)}^{m} = \beta_{(010)} - \beta_{(hkl)} = 1.2(3) - 0.43(6) = 0.8(2)$ Å^{-1}. This value and the very low intensity of the (010) peak (Figure 8b) suggest that the compositional fluctuations may be very important ($\delta \approx 0$) and the frequency of mistakes may be very high.

Concluding Remarks

The crystal structure of materials with complex microstructure effects needs to be studied by different complementary techniques, which allow one to detect and to treat the extended defects present in real solids.

SAED and HRTEM results of materials of the $La_{2/3-x}Li_{3x}TiO_3$ system indicate that they have a perovskite-related structure with unit cell dimensions $\sqrt{2}a_p \times \sqrt{2}a_p \times 2a_p$. Domains with different orientations of the unit cell form all of the crystals, and the size of the domains depends on the thermal treatment and the composition of the oxides.

These results have led us to consider the microstructure of the materials for determining their crystal structure. In this way, the crystal structure of three representative oxides of the system has been solved from synchrotron X-ray diffraction data. The high resolution of this technique has allowed us to distinguish between the monoclinic symmetry of the $La_{0.6}Li_{0.2}TiO_3$ quenched from 1000 °C and the orthorhombic symmetry of the $La_{0.55}Li_{0.35}TiO_3$ quenched from 1000 and 800 °C. All of the materials obey the same octahedral tilting mechanism, and ordering of the lanthanum and lithium ions and vacancies occurs along the $2a_p$-axis. This ordering depends on both the annealing temperature and the composition of the samples. However, location of the lithium ions must be obtained from neutron diffraction data. In addition, displacements of the titanium ions from the center of the TiO_6 octahedra are also observed.

We have also determined the average sizes and shapes of the domains of the three samples, and we have detected other microstructure effects such as strains and compositional fluctuations, which depend on both the thermal treatment and the sample composition.

Finally, it must be stressed that microstructural studies have valuable importance for the understanding and the optimization of the physicochemical properties of solids. Regarding the lithium ionic conductors $La_{2/3-x}Li_{3x}TiO_3$, the subject of this work, and other related systems,[22,23,50] we have found that the materials' performance as lithium conductors seems to be strongly dependent on the exact composition and on the microstructure. The oxides with the highest ionic conductivity in every system are those with 8% of vacancies within the A-sites in the perovskite structure and that are formed by microtwinned crystals. In this connection, some years ago Harada et al.[18] have reported that, among samples of $La_{2/3-x}Li_{3x}TiO_3$ of different compositions and thermal histories, those with high lithium content ($x \geq 0.09$) and that were annealed and quenched from high temperature (~1350 °C) present higher conductivity than those treated at lower temperature (800 °C). Interestingly, we have shown in this work that the samples with lithium content corresponding to ($x \geq 0.10$) annealed and quenched at high temperature present microtwins and a very defective microstructure as a consequence of high-density compositional mistakes within the microdomains.

Thus, high ionic conductivity in perovskite-like systems seems to be clearly related to the microstructure of the material, which can be modified by adjusting the composition and controlling the thermal treatments to which the material is submitted.

Acknowledgment. This study was financially supported by CICYT (Projects MAT2001-3713-C04-01 and MAT2001/1217) and USP-CEU (Project USP-7/01). Financial support from the Comunidad Autónoma de Madrid (Projects CAM25/2001-CET2001 and CAM07N/0052/2002), and MCYT (Spain) and DAAD (Germany) in the frame of "Acciones Integradas Hispano-Alemanas", is also gratefully acknowledged. This paper was inspired by a previous work of S.G.-M., in collaboration with Dr. A. D. Robertson and Prof. A. R. West; we are indebted to them for valuable suggestions, comments, and discussions. We thank Prof. H. Fuess for the careful reading of this manuscript and his suggestions, and also Dr. A. Várez and Dr. J. Sanz for valuable discussions. We thank the Microscopy Centre Luis Bru from U.C.M. for technical assistance.

Supporting Information Available: Schematic representations and a plot of $La_{0.55}Li_{0.35}TiO_3$ (PDF). This material is available free of charge via the Internet at http://pubs.acs.org.

JA038410L

(50) Morata-Orrantia, A.; García-Martín, S.; Alario-Franco, M. A. *Chem. Mater.* **2003**, *15*, 3991.